Journal of Design Against Fatigue
https://minerva-aset.com/JDAF
MINERVA ASET ISSN 2976-940X

Fatigue behavior in Inconel alloys produced by 3D printing: A short review

Kazem Reza Kashyzadeh [a]*, Siamak Ghorbani [b]

[a] *Department of Transport Equipment and Technology, Academy of Engineering, RUDN University, 6 Miklukho-Maklaya St., Moscow, 117198, Russian Federation.*
[b] *Department of Mechanical Engineering, Academy of Engineering, RUDN University, 6 Miklukho-Maklaya St., Moscow, 117198, Russian Federation.*

P A P E R I N F O

Paper history:
Received 25 April 2025
Received in revised form 21 may 2025
Accepted 31 May 2025

Keywords:
Superalloy, Inconel, Additive manufacturing, Fatigue, Heat treatment, Post-processing.

A B S T R A C T

Inconel alloys, especially IN625 and IN718, are widely used in the aerospace and energy industries due to their excellent resistance to high temperatures and corrosion. With development in additive manufacturing (AM), the production of complex geometries from these alloys, such as gas turbine blades, has become feasible. However, the fatigue performance of AM Inconel components is influenced by various factors including manufacturing methods, microstructure, heat treatment, and surface quality. This review investigates the key parameters affecting the fatigue behavior of AM-fabricated Inconel alloys. Findings highlight that heat treatment significantly alters microstructural characteristics such as grain size, texture, and precipitate distribution. Moreover, loading path and operational temperature impact crack propagation mechanisms. Post-processing techniques such as hot isostatic pressing enhance fatigue performance by reducing residual stresses, porosity, and microcracks, and improving surface finish and surface layers and high compressive residual stresses. Eventually, optimizing AM process parameters and applying appropriate post-treatments are essential to improving the fatigue life of Inconel alloys and ensuring their reliability in critical applications.

https://doi.org/10.62676/jdaf.2025.3.1.20

1. INTRODUCTION

Superalloys based on nickel are essential components used in the production of disks and blades in high-pressure turbines for gas turbine engines. In addition, they are employed in numerous cryogenic and high temperature applications, including manifolds, injectors, igniters, turbomachinery, and valves [1]. The efficiency of contemporary aircraft engines is significantly increased by their exceptional mechanical qualities in corrosive conditions, at extremely high temperatures, and under high pressures [2]. Manufacturing complex metal products using conventional methods like casting, forging, machining, drilling, and etc. presents substantial challenges and demands considerable resources throughout the production process. On the other hand, in different industries, such as automotive, robotics, aerospace and shipbuilding, the need for complex, multifunctional, and high-performance components is growing [3]. At present, additive manufacturing (AM) technology makes it possible to fabricate parts of various geometric shapes through layer-by-layer application of material onto a substrate or element of a finished product, based on a computer-aided design (CAD) model, which significantly reduces costs. For instance, devices for combustion injectors, combustion chambers, nozzles,

*Corresponding Author Email: reza-kashi-zade-ka@rudn.ru
(Prof. Dr. Kazem Reza Kashyzadeh)

Cite this article as: Kazem Reza Kashyzadeh, Siamak Ghorbani, Fatigue behavior in Inconel alloys produced by 3D printing: A short review, ***Journal of Design Against Fatigue,*** Vol. 3, No. 1, (2025), https://doi.org/10.62676/jdaf.2025.3.1.20

Copyright: © 2025 by the author(s). Published by Minerva ASET, Devon, UK. This is an open access article distributed under the terms and conditions of the Creative Commons Attribution (CC BY) License. (https://creativecommons.org/licenses/by/4.0/).

and augmented spark ignition systems are among the parts that are fully utilizing additive manufacturing [4]. Typically, in AM, a laser or an electron beam is used to (selectively) melt or sinter the feedstock. The materials used in additive manufacturing include metals, polymers, inorganic nonmetal materials and their components [5]. The production-development cycle is enhanced by AM technology. They are able to fabricate functionally graded parts as well as small batches of parts in a short time and with low financial investment [6-8]. Additionally, the better dimension accuracy and mechanical properties as well as freedom of design provided by AM techniques make them a suitable technique when producing components made of difficult-to-machine materials, including nickel-based superalloys (Inconels) [9]. The improved mechanical and microstructural properties of components produced by AM are mainly related to the rapid cooling by laser resulting in finer microstructure [10]. Significant tool wear and low material removal rates for room temperature machining and refractory element segregation (Nb and Mo) for high-temperature forming operations may make it difficult to fabricate Inconel components using traditional machining techniques. Complex Inconel components, including turbine blades with internal cooling channels or the many tiny nozzles of liquid rocket engine injectors, provide an even greater problem and necessitate the use of AM techniques [11]. In conventional thermomechanical processing of turbine part manufacturing, further post-processing techniques like machining are needed. Because of high hardness and tendency to work harden, which in turn require high cutting forces and result in higher work hardening effects, nickel-based superalloys like alloy 718 and 625 are very challenging to machine. Consequently, only around 10% of nickel based superalloys can become final products [12]. It is reported that, by applying AM for the GE integrated fuel nozzle, the weight is reduced by 25%, and the durability is improved in five times compared to the traditional assembly. This was mainly due to the reduced assembly operation from 20-part assembly made of cobalt chrome material to single component [13]. This may lead to a reduced risk and cost for multiple components and reduced potential failure modes across joints [14]. In addition, in AM nickel-based superalloy, increasing the solid solution strengthening elements within the commercial alloy composition range was found to reduce microcracking [15]. Further, AM reduces the buy-to-fly-ratio as low as 1:1. As it is the key identifier in aerospace and structural engineering, which is the ratio of the weight of purchased material to weight of finished part [16]. By reducing the amount of material needed, AM reduces costs by as much as 30 to 50% in comparison to traditional methods [17]. Process parameters during AM that can affect the quality and properties of the manufactured components include power, scan speed, hatch spacing or overlap between tracks, scan strategy (e.g., use of contours, angle changes of hatch tracks per layer), and many more [14]. The mechanical characteristics of as-built AM components and the possibility for defects to arise still provide a barrier to the development of this technology. Heterogeneous microstructure and anisotropic mechanical properties are the result of a variety of periodic microstructural and internal defect distribution characteristics AM methods, including pores, cracks, residual stresses, and weak interfaces [3]. Directional grain refinement fractures, residual stress, and pores are readily introduced by the uncoordinated deformation and incomplete contact of the solid and liquid contact surfaces, while the directional nucleation of the crystals produces extremely regular orientations during the cooling process. Metal anisotropy may be caused by the presence of directed temperature gradients in AM [3]. Moreover, other obstacles that AM must overcome are the intrinsic defects in AM processes, the lack of a substantial database for AM materials, and the lower fatigue resistance [14]. Premature mechanical failures are caused by the pores and hazardous phases, which act as stress risers, void nucleation sites under tension, and fatigue crack initiation sites under cyclic loading [18]. Insufficient knowledge in this field may cause the finished parts to fail too soon in addition to not utilizing AM technology's full potential benefits. In order to ensure that parts meet the intended design and metallurgical characteristics, the certification process must be decided early in the design process to include both a methodology and traceability throughout all stages of AM including the implementation of adequate non-destructive evaluation techniques, surface enhancements to improve fatigue performance, optimization of thermal processing, and other pre-build and post-processing operations. The methodologies require strict control of machine parameters, powder lots, and include a detailed understanding of variations in powder or off-nominal build operations [14]. Therefore, both industry and academics have become increasingly interested in AM technology in recent years. In this work, two Inconel alloys, namely IN625 and IN718, manufactured by AM are chosen to discuss the effect of production processes, microstructure, heat treatment, and surface imperfections on the fatigue behavior of Inconel alloys.

Although additive manufacturing of Inconel alloys has been extensively explored in recent years, there remains a fragmented understanding of how various AM methods affect the fatigue performance of these alloys. This short review is particularly timely due to the increasing industrial demand for reliable, fatigue-resistant Inconel components manufactured through AM techniques. Despite numerous publications on individual AM

processes, there is a lack of a consolidated study that compares their respective influence on defect formation, microstructure evolution, and fatigue behavior. The current article aims to bridge this gap by providing a comparative analysis of SLM, DED, WAAM, EBM, and LPBF processes with respect to their mechanical and microstructural implications on Inconel 625 and Inconel 718.

2. MATERIALS AND APPLICATIONS

Nickel-based superalloys (Inconels) primarily consists of nickel (Ni) and chrome (Cr) possess high mechanical properties including creep, corrosion, fatigue and oxidation resistances even at high temperatures and extreme environmental conditions [19]. Amongst the several nickel-based superalloys, the most widely used commercial alloys in the automotive, aerospace, and energy applications are Inconel 625 (IN625) and Inconel 718 (IN718). This is especially because of their outstanding thermo-mechanical qualities. Table 1 represents the chemical composition for both the alloys (IN625 and IN718).

Micromechanical characteristics of nickel-based superalloys mainly depends on temperature, composition, characteristics of dislocation slip systems and dislocation-interaction with precipitates [20]. From Table 1, there are various alloying elements in nickel-based superalloys, which form different precipitate and several phases including austenitic γ-grain nickel matrix, γ′ (Ni3Al), and γ″ (Ni3Nb) [21]. The strength of nickel-based superalloys at higher temperatures is mostly determined by the γ′ phase's morphology, size, and volume fraction [22]. The ordered crystal structure of γ′ and γ" phases in nickel-based superalloys prevent dislocations by increasing the energy needed for their movement and improving the material's overall strength and performance. Nickel-based superalloys are strengthened by solid solution when elements such as Cr, Fe, Co, Mo, W, Hf, Re, and Ru are present in the γ-grain matrix. On the other hand, elements including Al, Ti, Nb, and Ta have a tendency to separate and create ordered crystal structures in the form of Ni3Al (γ′) or Ni3Nb (γ″) precipitates [17]. This alloy, which is rich in Nb, Mo, and Cr, may also contain various forms of carbides in the forms of MC, M6C, and M23C6 [23]. Moreover, some undesirable phases, like needle/plate-like orthorhombic δ phase ((Ni3(Nb,Ti)), Laves and μ phases with topologically close-packed structures made up of more than ten elements, are also present in superalloys [20]. Because of their low solidus, these phases tend to solidify heavily, which can cause solidification cracking during AM operations. Properties, like fatigue performance, are significantly impacted by the phases in the superalloy matrix [24]. Figure 1 graphically depicts the typical microstructures produced in Inconel superalloys.

TABLE 1. Chemical compositions of IN625 and IN718 alloys in wt% [20].

Element	IN625	IN718
Ni	> 58	50-55
Cr	20-23	17-21
Fe	< 5	Balance
Nb	3.15-4.15	4.75-5.5
Mo	8-10	2.8-3.3
Mn	< 0.5	< 0.35
Al	< 0.4	0.2-0.8
Ti	< 0.4	0.65-1.15
Co	< 1	< 1

IN625 is a face-centred cubic solid-solution strengthened superalloy with outstanding resistance to oxidation, and microbiological and CO_2 corrosion, superior weldability, and mechanical characteristics that include creep and fatigue at elevated temperatures. As a result, the alloy is utilized at temperatures up to about 980 °C [25]. Because of these characteristics, IN625 is a great option for use in harsh environments, including nuclear and aerospace sectors, petrochemical, chemical and marine applications - structural components in the pre-salt industry [23]. The key properties of IN625 and IN718 are given in Table 2.

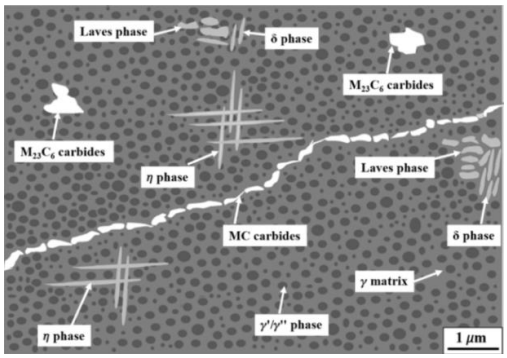


Figure 1. Schematic representation of microstructure of Inconel superalloys [20].

TABLE 2. Properties of conventionally manufactured IN625 and IN718 [26].

Properties	IN625(Rolled)	IN718(Rolled)
Tensile strength (MPa)	827-1103	1407
Yeild strength (MPa)	414-758	1172
Elongation (%)	30-60	6-12
Reduction of area (%)	40-60	8-15
Hardness Brinell	175-240	331
Density ($^{gr}/_{cm^3}$)	8.44	8.19
Modulus of elasticity (GPa)	207.5	199.9

The superalloy IN718 is a face-centred cubic niobium-modified precipitation hardened nickel–iron alloy, which has high concentrations of iron, niobium, molybdenum, and chromium. At extreme temperatures (up to 700 °C), this alloy demonstrates exceptionally high mechanical

qualities such as yield strength, tensile strength, creep rupture capabilities, superior fatigue life, good weldability [20]. IN718 is primarily utilized for complex aerospace components, including high-pressure pipes, thin-walled hollow blades, and turbine rotor discs [27]. The chromium contents in Nickel-based superalloys used in industrial gas turbine applications are higher. On the other hand, aerospace alloys for high-pressure turbine applications contain more refractory metals and less chromium. However, improved structural and oxidative properties have been observed for high-pressure turbine alloys [28]. At operating temperatures, the majority of superalloys based on nickel exhibit creep-brittleness. Wrought superalloys, however, are creep-ductile. Therefore, the wrought alloys are commonly employed for industrial gas turbine applications but are confined to disc applications as in high-pressure turbine. Only a small number of the superalloys created for gas turbine applications are used in turbine disc applications [21]. Further, resistance to fatigue-crack propagation, especially at service temperatures, is a crucial characteristic of nickel-based superalloys. When used in constructions like gas turbines and jet engines, many nickel-based superalloys are susceptible to the development of fractures or incipient cracks during fabrication or use. These cracks have the potential to propagate or grow under stress [29]. From Table 2, IN718 has better tensile strengths and lower elongation level compared to IN625, respectively.

3. INCONEL ALLOY ADDITIVE MANUFACTURING METHODS

AM techniques can be classified according to the type of feedstock (wire or powder) and the energy source (laser or electron beam) (see Figure 2). The required properties of the designed part, such as dimensional precision, microstructure, and mechanical performance, determine which AM process is suitable to fabricate the component [11]. Various metal AM techniques have been used for nickel-based superalloy, including selective laser melting (SLM), direct energy deposition (DED), wire arc additive manufacturing (WAAM), electron beam melting (EBM) and laser powder bed fusion (LPBF) [19]. The schematic representation of each mentioned AM technique is illustrated in Figure 3. The characteristics of the mentioned techniques as well as their effect on the microstructure and properties of nickel-based superalloys are discussed below.

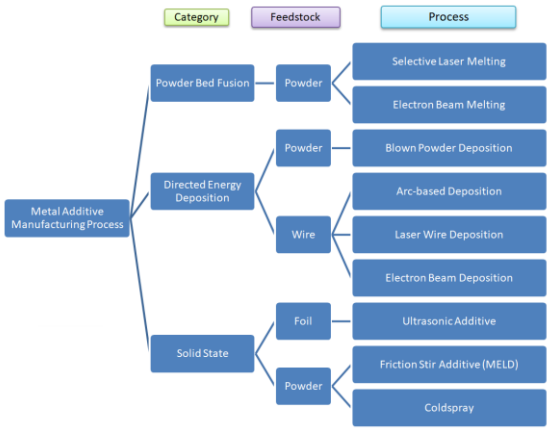
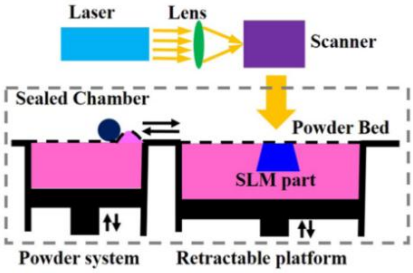


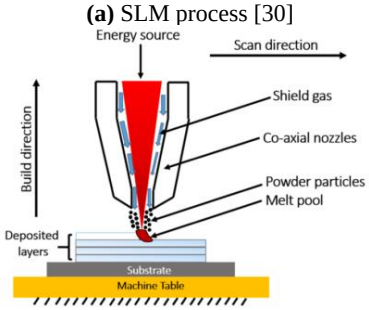
Figure 2. Metallic AM classification.

3.1. Selective Laser Melting: SLM

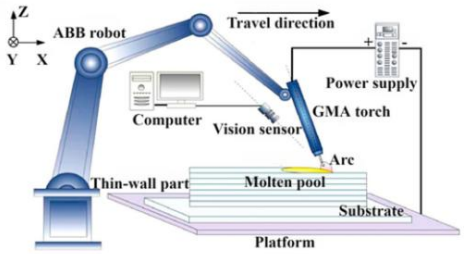
Selective laser melting is a part of the powder-bed fusion processes for manufacturing complex-shaped and structured products from metal powders using mathematical CAD models. SLM process involves sequential layer-by-layer melting of powder material using powerful laser beam (Figure 3 (a)). In order to minimize the oxidation of the raw material, the process is conducted in a chamber with an inert gas like argon or nitrogen [34]. SLM allows to fabricate metal products of high precision and multifaceted parts with a higher density up to 99.9% by melts the metallic powders via a high-power-density laser; to optimize the design and reduce the weight of the produced parts. SLM techniques are found to possess high quality and



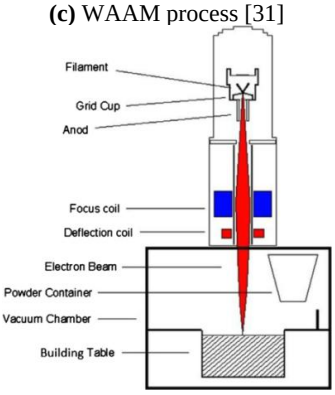
(a) SLM process [30]



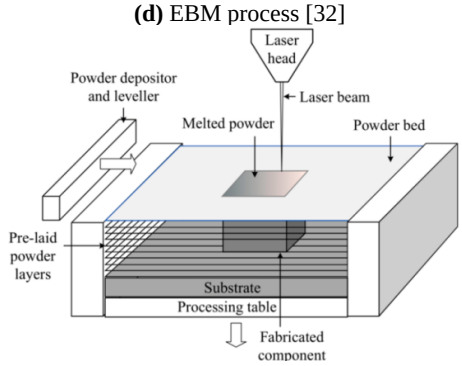
(b) DED process [20]



(c) WAAM process [31]



(d) EBM process [32]



(e) LPBF process[33]

Figure 3. Metal AM technologies for Inconel

exhibit desirable performance. In addition, component with a high resolution (10–200 µm) can be fabricated by SLM technique [35]. SLM can apply different materials including aluminium, iron, titanium-based, copper-based as well as nickel-based superalloys. SLM makes it possible to manufacture objects that surpass the physical and mechanical properties of products of standard technologies. This is related to the small diameter of laser beam, low laser power, high scan speed, and low value of heat input [19]. SLM technology makes it possible to create unique complex-profile products without the post-processing operation, like machining, and expensive tooling, in particular, due to the ability to control the properties of products. Moreover, SLM technique can help optimize the part's weight and reduce the number of assembly parts into a single component [36]. However, shrinkage and residual stress are important SLM process phenomena. During the procedure, the material is enlarged by the laser power, and it will contract once the laser power is removed. Furthermore, the use of incorrect process parameters also contributed to the residual stress and defects including porosity, incomplete fusion holes, and cracks [37].

3.2. Directed Energy Deposition: DED

The working principle of DED represented in Figure 3(b). By focusing a high energy density heat source, such as a laser, electron beam, or plasma/electric arc, on the substrate, DED forms a small melt pool and melts the feedstock material that is delivered into the melt pool in the form of wire or powder. A metal track is created when the deposited metal hardens on the substrate as the heating source advances. According to the predetermined hatch spacing—that is, the separation between consecutive metal tracks—the metal tracks overlap one another. When a layer is finished, the feedstock delivery system and the deposition head shift upward by a tiny amount (slice thickness) to deposit the subsequent layer [38]. DED can process various range of feedstock materials, multi-materials, composites and functionally graded materials. DED provide better static and dynamic mechanical properties in the as-deposited condition in comparison with powder bed fusion deposited parts. DED uses larger powder particle sizes with laser compared to powder bed fusion with laser leading to less cost and better safety. Higher material deposition rate can be provided by DED, though this method is suitable for the economic production of large metallic components [39]. DED is extensively utilized in the military, medical, and aerospace sectors due to the great degree of design freedom that can be attained with this technology. Nonetheless, the construction components typically have comparatively low dimensional accuracy and surface quality [19]. During DED the layers deposited along their corresponding curved layer bonds are apparent at the macroscale. As the flow rate of the metallic powder increased, the surface roughness value of the DED parts increases as well. Furthermore, the mean surface roughness in the DED process may be significantly influenced by the manufacturing method used for the powder material [26].

3.3. Wire Arc Additive Manufacturing: WAAM

WAAM used arc power as the heat source. Its heat source is 1/10 and 1/30 of the laser transmitter and electron beam generator, respectively. Therefore, it leads to better efficiency and a bigger advantages in economy specially in large-scale industries [40]. Products based on WAAM have considerably superior mechanical and metallurgical properties and a higher metal wire deposition rate (15–130 gr/min) to those of standard additive manufacturing [31]. The mechanical and metallurgical properties of

material produced using WAAM can be further enhanced by post-processing procedures [41]. These characteristics make the WAAM an ideal method to fabricate medium-/large-scale component manufacturing in small batches with near-net shapes in the energy, automotive, aerospace (wing ribs and stiffeners, landing gear parts), and construction, defense, plant and refineries and other industries for small batch near-net-shape fabrication of medium- and large-scale components [31]. The WAAM technology creates the necessary part by layer-by-layer material deposition [42]. As can be seen in Figure 3(c), the main elements of WAAM are illustrated including an electric arc as the heat source shielded by inert gas, a wire consumable as the feedstock, a robotic arm or gantry machine as the manipulator that is precisely controlled by a computer system, and the sequential deposition of metal layers in either a controlled chamber or an open environment [31]. The electric arc in WAAM is produced using plasma arc welding (PAW), gas metal arcwelding (GMAW), and gas tungsten arc welding (GTAW). GMAW is a good option for producing superalloy, because of its extremely fast rate of deposition, automation potential, and appropriate inert gas shielding for the weld metal [19].

3.4. Electron Beam Melting: EBM

As seen in Figure 3(d) the EBM system consists of a 60 kW electron gun that produces a concentrated beam with an energy density of over 100 kW/cm^2. Electromagnetic lenses control the beam's focus, and deflection coils control the beam's movement on the build table. To build a part, a 100 micron-thick layer of powder is spread across the table, from two hoppers stored inside the build chamber. A moving rake collects powder from both sides and spreads it across the table. In EBM, each layer of a part is constructed in two steps: the outer boundary of the part is constructed first, known as contouring, and the powder inside the contour is melted later to complete one layer. The electron beam first pre-heats the powder layer with a higher scan speed, then melts the powder layer based on the geometry specified by the CAD file. This process keeps going until the necessary three-dimensional component is completed. A high vacuum is maintained during the entire operation [32]. Although electron beam melting (EBM) produces components that are fully dense, void-free, and incredibly strong, the products are often smaller than those made by laser. The EBM process could be used to make nuclear component materials in nickel-based alloys, however a cost-benefit analysis should be conducted to ascertain the feasibility in comparison with existing fabrication methods. Because of their high densification and working temperature, which is usually 700–1000 °C during the fabrication process, EBM-fabricated components don't need to be heat treated [43]. Moreover, there may be considerable porosity in the EBM samples, which reduces fatigue and stress rupture life [44].

3.5. Laser Powder Bed Fusion: LPBF

LPBF is a powerful AM technique that can create metal objects with a high degree of geometric complexity with near full density (>99%) and freedom. Layers of metal powder particles are melted and fused together by LPBF using a direct laser beam (see Figure 3(e)). The remaining extra powder will be eliminated until the required shape, according to the CAD data, is reached. The excess powder is a suitable option for recycling since it can be recycled for future use. The alloy's microstructure and characteristics are typically anisotropic due to the significant temperature differential and complex heat transport caused by laser beam cyclic processing, and new metastable or even amorphous phases may form. For the formation of small batch, high-value, customized, and complicated structural parts for automotive, biomedical, and aerospace applications, LPBF is particularly well-suited [33]. Because laser melting is used in LPBF, materials with high melting points and hardness, such as nickel-based alloys, can be handled rapidly. The hardness, yield, and ultimate strength of metal parts (in particular IN718) can be improved by the LPBF's adjustable microstructure, which can be controlled by process parameters. Its performance is comparable with or even greater than that of forged or cast IN718 alloy. Furthermore, epitaxial growth in IN718 allows the LPBF technique to create distinct crystallographic textures, resulting in anisotropy in mechanical strength. The production of single-crystal-like, lamella, and poly-crystal microstructures in IN718 leads to strengthening through the texture effect [45]. However, defects in LPBF are common because of the high residual tension caused by the high-intensity contact between the laser beam and the powder layers. Cracks, layer delamination, distortions, and porosity are examples of part defects that can compromise the performance and quality of 3D parts [46].
A comparative summary of AM techniques regarding defect types, microstructure, and fatigue performance is presented in Table 3.

TABLE 3. Comparative summary of AM techniques used for Inconel alloys

Technique	Defect types	Microstructure features	Fatigue performance
SLM	Porosity, lack of fusion, and residual stresses	Fine grains, columnar dendrites, and anisotropy	Moderate – improved by post-processing
DED	Surface roughness and large	Coarse grains and less residual stress	Better than SLM in some conditions

WAAM	melt pool defects Oxide inclusions and distortion	Columnar grains and large grain size	Lower without post-processing
EBM	Porosity and rough surface	Equiaxed grains due to high temperature	High, no need for heat treatment, but small parts
LPBF	Cracks, delamination, and porosity	Anisotropic and high cooling rate-induced texture	High (with heat treatment)

4. FATIGUE BEHAVIOR IN PRINTED SAMPLES

Wöhler's diagram, specifically the S-N curve in Figure 4, which links the applied cyclic stress amplitude σ_a to the fatigue life N, can be used to characterize the fatigue performance of materials. The inset of Figure 4 also shows the link between the maximum and minimum stresses for a sinusoidal load wave and the stress amplitude. Based on the fatigue life time, three zones can be identified from the S-N curve [47, 48]. In region I, the stress typically surpasses the yield strength of materials y, and the fatigue life is less than 10^4. Thus, plastic deformation—also known as low cycle fatigue (LCF)—dominates the fatigue life [49]. The fatigue life in region II is 10^7, and the stress is consistently less than σ_y. In other words, stress regulates fatigue life and the materials deform elastically [50-52]. High cycle fatigue (HCF) is the term used to describe this phenomenon. The fatigue life of nonferrous alloys diminishes with increasing stress amplitude beyond 10^7 (region III), approaching an asymptotic line known as the fatigue limit [24].

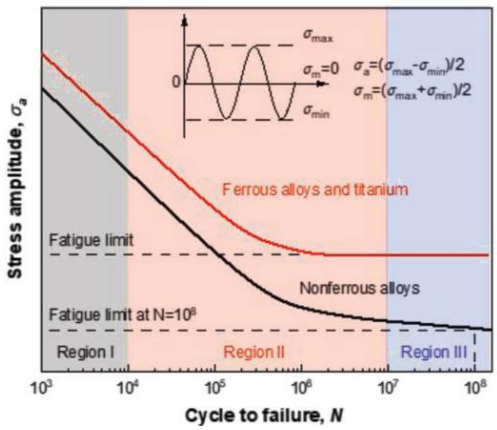


Figure 4. S-N Wöhler's diagram [24]

After a sufficient number of fluctuations, cyclic damage during the fatigue process leads to fracture and local cracking. Pores may greatly affect the fatigue behavior by creating stress concentrations at their walls. Fatigue failure is mostly a local phenomenon caused by impurities and microstructural heterogeneity, which are characteristics of metallic components produced with AM technology, as opposed to failures that happen under static loads [53]. It is commonly known that pre-existing defects (voids, dents, embossments, cracks, etc.) in metals and alloys, particularly those on the surface or near-surface, second phase or inclusions, grain boundary, or phase boundary, are the main factors influencing fatigue behavior. The microstructure's influence on fatigue performance mostly affects how cracks occur. Grain-level plasticity is localized in persistent slip bands caused by the polycrystal's repetitive deformation, and these bands eventually degenerate into microscopic fatigue cracks. These bands and subsequent cracks are more likely to occur in areas of the microstructure that correspond to the locations where a variable associated with cyclic plastic deformation is localizing [54]. Micromechanical models that simulate these mechanisms must be utilized in order to take into account the impact of the microstructures produced by AM on the prediction of fatigue life. When examining the fatigue performance of metal parts fabricated by AM, it should be taken in account the main factors such as surface roughness, printing defects, residual stress, and microstructure characteristics [27]. Because fatigue failure of materials is, in fact, an interaction result of multiple elements, including the size, volume fraction, and morphology of process-induced defects as well as microstructural characteristics, it can be difficult to comprehend and interpret. Due to their unique properties, such as high cooling rates during layer-by-layer material deposition, which result in notably different microstructure and defect features compared to those of wrought processes, AMed processes may even make it more difficult to interpret the fatigue failure of materials. Fatigue resistance are directly related to the microstructural features of the part and can be adversely affected in the presence of tensile residual stresses. However, it has been discovered that the primary cause of the greater scatter in high cyclic fatigue (HCF) data of AM materials is the location, size, and shape of voids [55]. By considering the roughness valleys as periodic fractures, the surface roughness effects can be examined in terms of the $\sqrt{area_R}$ parameter, which considers the effects of the roughness valleys' height and pitch [56]. Murakami et al. [57] established a grading system for AM materials based on the ratio of the apparent and ideal fatigue limits (determined by the hardness). They discovered that specimens without post-process treatments were placed in the fatigue worst grade, where the fatigue limit only corresponds to 10–30% of the ideal fatigue strength. Liu et al. [27] carried out a tension–compression fatigue testing with stress ratio $R = -1$ and loading frequency of $100\ Hz$ to study the relationship between microstructure, defects, and materials properties (e.g., hardness and tensile strength), with fatigue

performance of IN718 prepared by SLM. Four types of fatigue crack initiation was illustrated, including lack of fusion defect-deduced crack initiation on the surface (Figure. 5 (a) and (b)), crystallographic facet-induced secondary crack on the subsurface (Figure 5 (c) and (d)), multiple lacks of fusion defects-assisted crack initiation on the surface (Figure 5 (e) and (f)), and microstructural inhomogeneities such as columnar dendrite (Figure 5 (g) and (h)). The fractured surface showed the three typical stages of crack initiation, crack propagation, and overload fracture upon cyclic loading, as shown in Figure 5 (a) to (g). The authors concluded that, defects based on optical microscope measurements of the bulk materials and analysis of SEM fatigue crack sources using a combination of the Murakami model and extreme value statistics might be used to predict the fatigue limit.

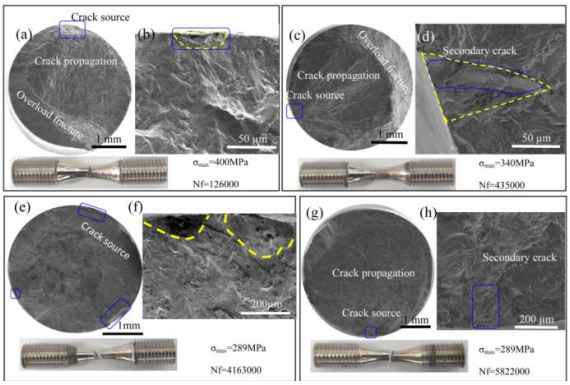


Figure 5. Fracture morphologies of the IN718 SLM samples after fatigue failure: (a), (b) lack of fusion defect; (c), (d) crystallographic facet; (e), (f) multiple lack of fusion defects; (g), (h) microstructural inhomogeneities [27].

Li et al. [58] performed the axial fatigue tests with stress ratios of -1 and 0.1 at 650 $^{\circ}C$ to examine the fatigue failure mechanism of a nickel-based superalloy manufactured by SLM in the long life regime at high temperature. They presented the interior cracking mechanism of SLM nickel-based superalloy (Figure 6). From Figure 6, when twin boundaries and metallurgical defects are present, the oxidate layer's inhibition effect promotes the nucleation of interior cracks and is strongly related to the accelerated dislocation movement and slipping within the interior grains that are situated in the highest shear stress plane. The rough crack morphology with a noticeable deflection phenomenon within the circular rough area (CDA) is caused by the change in grain orientation. Furthermore, lengthy interior crack propagation begins with the creation of CDA.

Koutiri et al. [59] studied the fatigue behavior of SLM manufacturing of Inconel 625 samples with a load R-ratio equal to -1. Both polished and as-built specimens have been the subject of an experimental fatigue campaign. The S-N Wöhler curve is shown in Fiugre 7. The authors stated that because heat concentration in the lower sides of SLM walls causes higher inclinations to raise average temperatures, the inclination of parts (between 10 and 35°) also clearly affects densification rates. The polished and as-built fatigue batches show comparable fatigue strength, despite the as-built specimen's poor surface roughness. The faults associated to fracture start locations, which are comparable in size for the specimens under study, can account for this. The same defect size seen at the initiation sites for the two batches under study explains this small discrepancy.

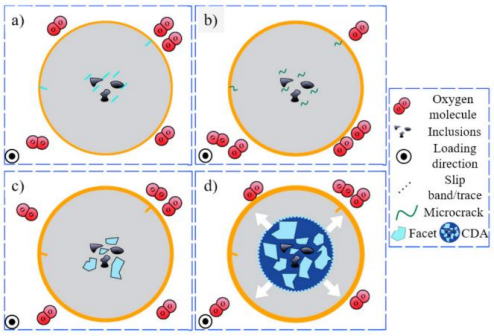


Figure 6. Schematic representation of interior cracking mechanism, including (a) Intensified slip lines or bands and oxide layer thickening; (b) Nucleation of microcrack; (c) Formation of facets and crack deflection; (d) Formation of CDA and subsequent long crack growth [58].

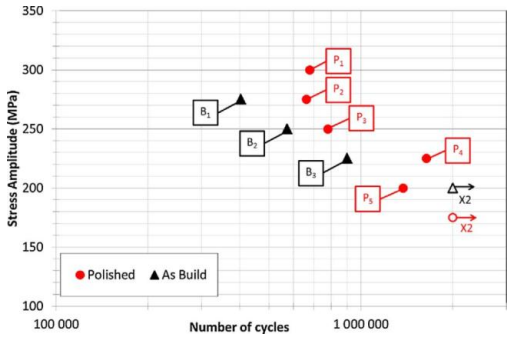


Figure 7. S-N Wöhler curves for polished and as-built batches of Inconel 625 made by SLM [59].

Bemfica et al. [9] studied the fatigue behavior of IN718 produced by SLM at room (20°C) and elevated temperature (450°C). The authors carried out strain-controlled axial and torsional (proportional situation) tests with $R_{\varepsilon} = 0$ fatigue lives ranging from 10^3 to 10^5 cycles. It was concluded that SLM IN718's fatigue crack propagation mechanism is dependent on temperature and loading path. Cyclic cleavage was the predominant mechanism under axial loading at both temperatures, while a classical transgranular mode with striations was observed at 20°C under torsional and proportional loading, and both striations and cleavage-like propagation modes were observed at 450°C. As shown in

Figure 8, the fatigue endurance of SLM Inconel 718 is inferior to its forged counterpart, especially at 450°C. A thirteenfold difference in fatigue life was noted for the greatest significant difference under torsional loading at 450°C.

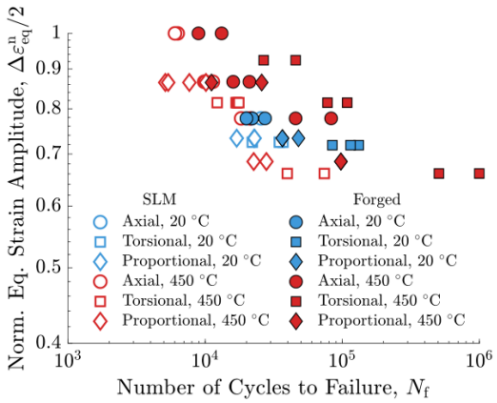


Figure 8. Equivalent strain-life data at 20°C and 450°C for SLM and forged IN718 [9].

The fatigue behavior of the IN625 manufactured by DED was described by Maciel [60]. Four point bending fatigue tests were conducted with varying load levels in order to achieve the S-N curve. Furthermore, the S-N curve obtained experimentally was compared to curves from the literatures as shown in Figure 9 [23, 59, 60-66]. Given that tensile mean stresses significantly reduce fatigue life, S-N curves derived from experiments with negative load ratios generally offer higher fatigue life for the same stress level. In this regard, $\sigma_{max} = -\sigma_{min}$ is implied by load ratio of -1, thus compressive stresses tend to prevent crack formation while tensile stresses encourage it, thereby promoting crack closure. The tested specimens' preliminary fatigue strength by DED was found to be greater than most of the data for SLM, indicating the reliability of the DED process's manufacturing and even its parametrization.

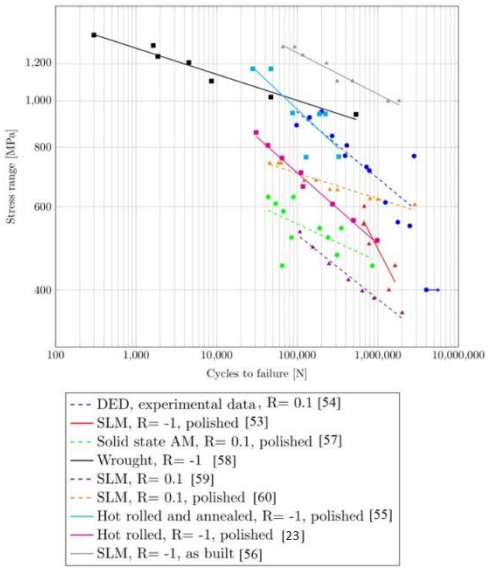


Figure 9. Comparison of S-N curves of IN625 produced by DED and SLM [60].

Wu et al. [67] studied the fatigue behavior of IN718 WAAM process analysed in both building direction (BD) and wall length direction (WD), utilising cold metal transfer (CMT). The S-N curve for BD and WD of the WAAM IN718 samples is demonstrated in Figure 10. The analysis showed that BD had better ductility than WD. The WD's fatigue endurance test revealed a longer lifespan than the BD's, which was explained by the BD specimens' greater stress concentrators. Examining a fractured specimen, however, revealed that the fatigue crack spread more quickly in the WD than the BD. However, Salvati et al. noted that because SP introduces unequal residual stress as a function of depth, it negatively affects the crack resistance of AM Nickel-base 718 alloy [68].

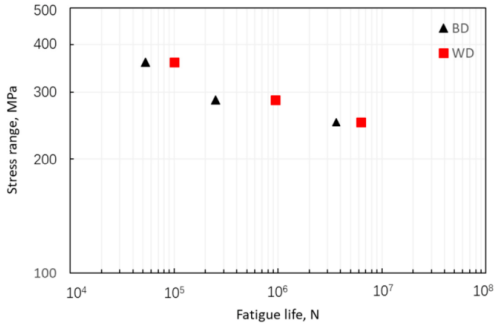


Figure 10. Comparison of fatigue behavior in different directions [67].

5. EFFECTS OF HEAT TREATMENT AND POST-PROCESSING

Surface roughness, internal defects (pores and fractures), microstructures, and residual stress all have a significant

impact on the fatigue performance of AMed alloy, which are impacted by a variety of factors due to AM's intrinsic characteristics. Fatigue mitigation techniques can be categorized into post-process treatment, inter-process control, and pre-process procedure [24]. Heat treatment and surface machining can further enhance AM Inconel 718's fatigue behavior, producing fatigue lifetimes that are comparable to those of wrought Inconel superalloys [9]. The microstructure, including the size, texture, grain mode, and precipitates, is significantly impacted by heat treatment. Annealing heat treatment can help reduce residual stresses and microstructural defects, improve the mechanical properties of the material, and increase its durability and resistance to failure. The annealing temperature and time depend on the type of material used and the desired mechanical properties. Annealing is frequently used in conjunction with other finishing techniques like machining, polishing, and surface treatment.

5.1. Hot Isostatic Pressing (HIP)

By subjecting the part to high pressure and temperature, hot isostatic pressing (HIP) can be utilized to increase hardness, remove residual stresses, decrease porosity, inclusions, and microcracks and improve surface finish and appearance. A denser and more homogeneous microstructure is produced by the high temperature encouraging plastic deformation and defect heal and the high pressure forcing the gas to diffuse out of the part. Because aging homogenizes the part's microstructure, it can enhance mechanical qualities including strength, toughness, and ductility. Additionally, the treatment might lessen the part's residual stresses, which may be the source of cracking or deformation [69]. Standard heat treatment for AM-processed parts typically includes an aging treatment to produce strengthening precipitates and a solution treatment to homogenize the microstructure and remove residual stress [24]. The ultra-high cycle symmetric bending fatigue performance of IN718 as-SLM and heat-treated specimens in the 300–800 MPa stress range is displayed in Figure 11, and the Basquin equation is used to match the S-N curve [70]. In addition, details of multi-step treatment are listed in Table 4. It was observed that, in comparison to the deposited condition (1.02×10^7), the SLMed IN718 alloy's fatigue life with a 300 MPa stress amplitude is noticeably longer following heat treatment (8.41×10^7 cycles ~ 3.64×10^8 cycles) and a complete machined process. Because the Laves phase, needle-like δ phase, and MC are eliminated (as seen in Figure 12), the fatigue life of HT-2 treated specimens is greatly increased at the same stress amplitude.

TABLE 4. Heat treatment of SLMed IN718 [70].

No.	**Heat treatment** (AC: Air cool, FC: Furnace cool, WC: Water cool)
HT-1	960 ℃ × 1 h(AC) + 720 ℃ × 8 h(FC) + 650 ℃ × 6 h(WC)
HT-2	1150 ℃ × 2 h(AC) + 960 ℃ × 1 h(AC) + 720 ℃ × 8 h(FC) + 650 ℃ × 6 h(WC)
HT-3	1150 ℃ × 2 h(AC) + 960 ℃ × 1 h(AC) + 650 ℃ × 6 h(WC)

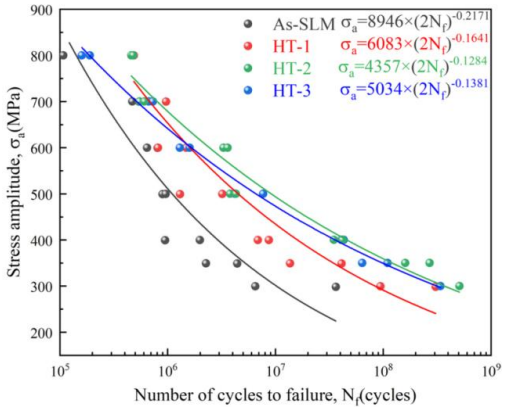


Figure 11. Comparison of HCF properties of SLMed IN718 alloy after different heat treatments under fully reverse loading at room temperature [70].

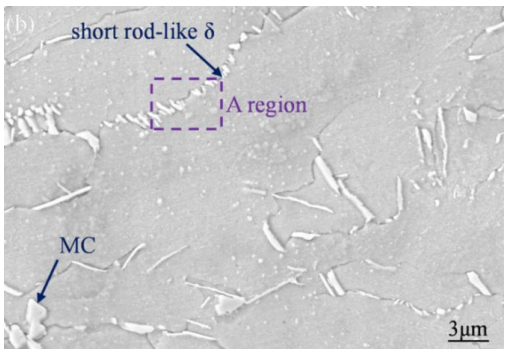


Figure 12. SEM microstructure of SLMed IN718 after HT-2 heat treatment [70].

Some authors stated that, since the $\frac{da}{dN}$ curves (a and N represent crack length and number of load cycles) following homogenization + solution annealing + direct ageing heat treatments resembled those obtained for the wrought material, heat treatment can also improve the fatigue crack growth behavior of AM Inconel 718 [71, 72]. Moreover, the high temperature and extended heat treatment period would eliminate more residual stress from SLM-processed IN718 alloy, according to Deng et al. [73]. Paranthaman et al. [74] showed that heat treatment enhanced the microstructure and mechanical properties of IN625 made by WAAM. Murr et al. [75] studied the effect of HIP on the mechanical characteristics of IN625 produced by EBM. It was indicated that while yield strength reduced from 0.33 to 0.30 GPa and UTS declined by 23%, the tensile characteristics of EBAM cylinders at 538°C did not

substantially change the microhardness of as-fabricated cylinders tested at ambient temperature. The corresponding elongation increased from 44% to 53%. Comparing tests at room temperature to those conducted at 538°C, the manufactured and HIP-ed cylinders showed no significant change in microhardness, while both yield strength and UTS decreased with little increase in ductility. In contrast, the wrought nickel superalloy that was tested at 538°C showed a UTS of 830 MPa and a yield strength of 280 MPa. Hu et al. [76] studied the effect of various heat treatments on the microstructural evolution and tensile properties of IN625 prepared by DED using the solution treatment (ST), solution + aging treatment (SA), and HIP treatment. From Figure 13 the microstructure of the as-deposited Inconel 625 was primarily composed of epitaxially grown columnar grains, with the chain-like Laves phase formed in the inter-dendritic regions.

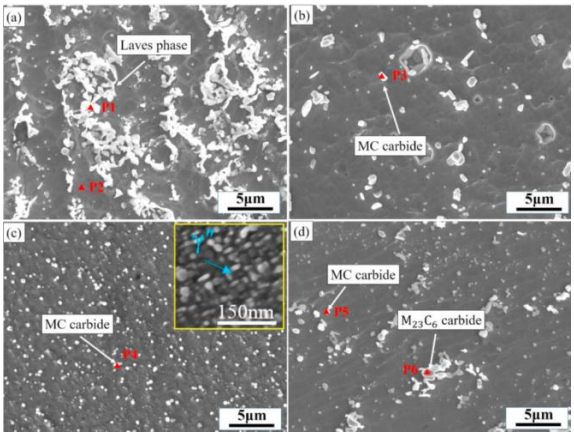


Figure 13. SEM images of the IN625 samples fabricated by DED: (a) As-deposited; (b) Solution treated; (c) Solution + Aging treated; (d) HIP treated [76].

The initial columnar grains were replaced by equiaxed grains during the high temperature heat treatment process due to the occurrence of static recrystallization, and the Laves phase fully dissolved into the matrix. The nanoscale γ″ phase formed after aging treatment, and both yield and ultimate strength were greater than those of the other samples. Tanvir et al. [77] stated that the annealing of IN625 produced by WAAM improved the ultimate tensile strength by 5% due to the precipitation and subsequent increase of the δ phases and MC carbides at the grain boundaries. In addition, HIP has been widely used for the densification of LPBF IN625 specimens, however it is limited to metallurgical pores that are not connected to the material surface. HIP has been demonstrated to increase fatigue life, but it significantly decreases mechanical strength in comparison to fully heat-treated specimens. This can be attributed to the partial recrystallization and dissolution of hard phases [78].

5.2. Surface Treatment Methods

Different types of surface treatment includes normal machining process, ultrasonic-assisted abrasive-belt-ground (UAABG), ultrasonic nanocrystal surface modification (UNSM) treatment, shot peening (SP), ultrasonic peening milling (UPM), and surface mechanical attrition treatment (SMAT) [24]. Due to high temperatures and grinding forces, which typically result in thermal damage to the workpiece, certain high-temperature nickel-based superalloys are difficult to machine. As a result, UAABG is applied to reduce grinding force and temperature, and improve surface integrity and fatigue performance [24]. Karimbaev et al. [79] studied the effect of UNSM treatment at room temperature and high temperatures (RT and HT) on the fatigue performance and mechanical properties of IN718 made by DED. At RT and HT, UNSM treatment significantly improved fatigue performance by approximately 43% and 57%, respectively (Figure 14). This is explained by the creation of a nanostructured surface layer and the introduction of a high compressive residual stress (CRS). From Figure 15 after UNSM treatment at RT and HT, the untreated sample's surface roughness dramatically decreased, which is crucial for preventing surface fracture initiation. By examining the fatigued surfaces, it was discovered that the primary fracture start location for the UNSM-treated samples was at the subsurface, but for the untreated ones, it was at the top surface. A crack initiation site was moved into the subsurface by the introduction of a high CRS by UNSM treatment at RT and HT.

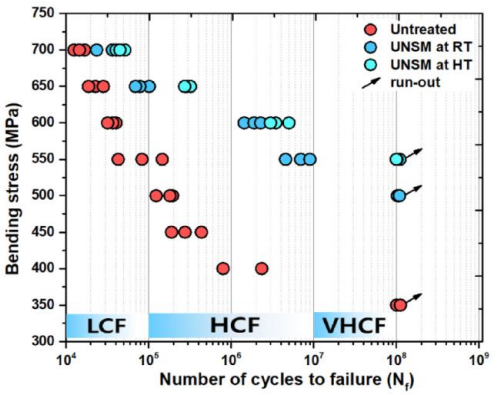


Figure 14. Comparison in S–N data of the untreated, UNSM-treated at RT and HT samples [79].

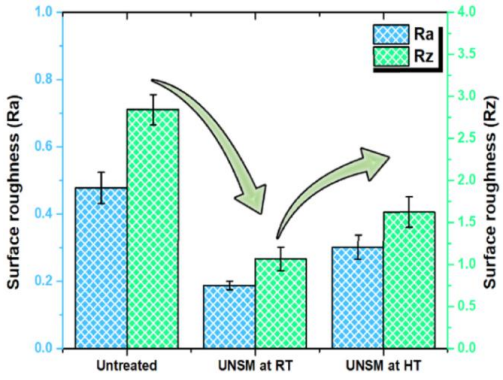


Figure 15. Comparison in surface roughness of the UNSM-treated and untreated samples at RT and HT [79].

Yin et al. [80] claimed that because of the significant improvement in the specimen surface integrity quality—such as the high CRS distribution, high surface microhardness, and degree of plastic deformation— the UPM considerably improves the fatigue life of the IN718 produced by SLM. With UPM, the CRS changed from -229 to -819 MPa, the cross-section hardness layer deepened from 65 to 80 mm, and the surface microhardness rate increased from 52.08% to 73.51%. Lesyl et al. [81] studied how the porosity and residual stress of the IN718 produced by SLM are affected by barrel finishing (BF), shot peening (SP), ultrasonic shot peening (USP), and multi-pin ultrasonic impact treatment (UIT).

5.3. Comparative Evaluation of Post-Processing Effects on Fatigue Performance

From Figure 16, following the BF, SP, USP, and UIT procedures, the porosity magnitudes were reduced by 23.1%, 40.6%, 55%, and 84%, respectively, in comparison to the residual porosity of the SLM-built specimen (0.697%). The near-surface layer's residual porosity (0.118%) was considerably decreased by the UIT procedure. The SLM-built specimen's tensile stresses (+120 MPa) were successfully converted into compressive stresses with the use of the BF (−201.4 MPa), USP (−313.8 MPa), multi-pin UIT (−428.7 MPa), and SP (−510.7 MPa) processes (Figure 17). Goksecaya et al. [45] applied three different electro-discharge machining strategies (rough, semi-finish, and finish cutting) on IN718 produced by LPFB and decreased the material removal rate and surface roughness, due to the the large grain size and less amount of grain boundary, while increasing cutting speed from rough cutting to finishing cut, as well as displayed less residue on the machined surface, leading to a better fatigue performance.

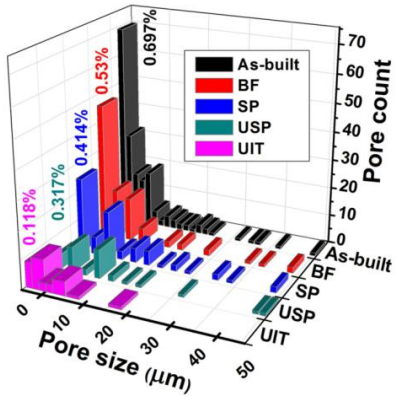


Figure 16. Relative porosity in the build direction of the SLM-built and BF, SP, USP, and UIT processed IN 718 specimens [81].

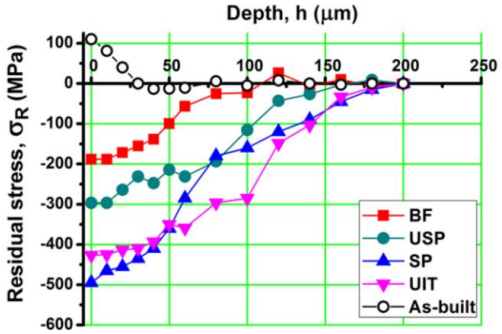


Figure 17. Residual stress depth profiles formed in the build direction of the SLM-built and BF, SP, USP, and UIT processed IN718 specimens [81].

6. CONCLUSION

Inconel superalloys, especially IN625 and IN718, have gained substantial attention due to their exceptional high-temperature strength and corrosion resistance, making them prome candidates for critical aerospace and energy components. This short review systematically explored the fatigue behavior of these alloys manufactured through various AM techniques.

The findings reveal that manufacturing-induced defects such as porosity, residual stresses, surface roughness, and heterogenous microstructures significantly affect fatigue life. Studies consistently show that as-built AM components generally exhibit inferior fatigue performance compared to wrought counterparts, particularly due to lack of fusion and internal cracks. However, post-processing treatments such as HIP, annealing, stress relief, and surface modifications can mitigate these issues by improving microstructural uniformity and reducing defect severity.

Contrasts among techniques were noted: DED-produced IN625 showed higher preliminary fatigue strength that many SLM-fabricated samples, suggesting process reliability. Meanwhile, WAAN-fabricated IN718

exhibited direction-dependent fatigue behavior, with crack initiation and propagation varying along different axes.

This short review also highlighted that SLM IN718, despite its anisotropic properties, can achieve comparable fatigue life to forged alloys after optimal heat treatment, as shown by the extension of fatigue life up to 8.41×10^7 cycles with HT-2 treatment. Moreover, surface treatment methods like UNSM and UPM significantly improved fatigue resistance by inducing high compressive residual stress and refining surface integrity.

Overall, the fatigue performance of AM Inconel alloys depends heavily on the interaction between process-induced defects and microstructural features. Harmonizing process parameters, material selection, and post-treatment protocols is crucial for realizing the full potential of AM in high-performance applications.

Despite significant progress in understanding the fatigue behavior of AM-fabricated Inconel alloys, several critical gaps remain. Future studies should address the following:

- Quantitative modeling of defect–fatigue relationships: While many studies have reported the detrimental effects of defects (e.g., pores, lack of fusion, surface roughness), comprehensive predictive models linking defect characteristics to fatigue life under multiaxial and variable loading conditions are still lacking.
- Standardization of AM processing parameters: Inconsistencies in reported fatigue data often stem from variations in AM process settings. Research is needed to establish standardized processing windows for different AM techniques specific to Inconel 625 and 718.
- High-temperature fatigue under service-like environments: Most experimental studies are performed at room temperature. Future work should focus on the fatigue performance of AM parts under real service conditions, including elevated temperatures, oxidation, and thermal cycling.
- Long-term performance of post-treated components: Although post-processing methods like HIP and UNSM improve fatigue resistance, their long-term effects on microstructure stability and mechanical performance require further investigation.
- Development of non-destructive evaluation (NDE) techniques: Innovative NDE methods are necessary to reliably detect internal defects and residual stress distributions in complex AM parts before deployment.

ACKNOWLEDGMENT

This paper was supported by the Russian Science Foundation (RSF, Grant No. 25-29-00536).

CONFLICTS OF INTEREST

The authors declare that they have no known competing financial interests or personal relationships that could have appeared to influence the work reported in this paper.

REFERENCES

1. K. Minet, A. Saharan, A Loesser, N. Raitanen, 8 - Superalloys, powders, process monitoring in additive manufacturing, Editor(s): Francis Froes, Rodney Boyer, Additive Manufacturing for the Aerospace Industry, Elsevier, 2019, 163-185, https://doi.org/10.1016/B978-0-12-814062-8.00009-1.
2. M. Perrut , P. Caron, M. Thomas, A. Couret, High temperature materials for aerospace applications: Ni-based superalloys and γ -TiAl alloys, C. R. Physique, 19 (2018) 657–671, https://doi.org/10.1016/j.crhy.2018.10.002.
3. S. Dai, K. Zhu, S. Wang, Z. Deng, Additively manufactured materials: A critical review on their anisotropic mechanical properties and modeling methods, J. Manuf. Process. 141 (2025) 789–814, https://doi.org/10.1016/j.jmapro.2025.02.038.
4. P. Gradl, S.E. Greene , C. Protz, B. Bullard, J. Buzzell, C. Garcia, J. Wood, K. Cooper, Additive manufacturing of liquid rocket engine combustion devices: a summary of process developments and hot-fire testing results, 54th AIAA/SAE/ASEE Joint Propulsion Conference 2018, Cincinnatti, OH United States Start, AIAA, ASEE, SAE, (2018), 1–34.
5. D. Bourell, J.P. Kruth, M. Leu, G. Levy, D. Rosen, A.M. Beese, A. Clare, Materials for additive manufacturing, CIRP Ann. Manuf. Technol. 66 (2017) 659–681, http://dx.doi.org/10.1016/j.cirp.2017.05.009.
6. A. Hinojos, J. Mireles, A. Reichardt, P. Frigola, P. Hosemann, L.E. Murr, R.B. Wicker, Joining of Inconel 718 and 316 Stainless Steel using electron beam melting additive manufacturing technology, Mater. Des. 94 (2016) 17–27, http://dx.doi.org/10.1016/j.matdes.2016.01.041 .
7. J.B. Roca, P. Vaishnav, E.R.H. Fuchs, M.G. Morgan, Policy needed for additive manufacturing, April 5, 2016, Available at

SSRN: https://ssrn.com/abstract=2759594, or http://dx.doi.org/10.2139/ssrn.2759594.

8. X. Wang, K. Chou, Electron backscatter diffraction analysis of Inconel 718 parts fabricated by selective laser melting additive manufacturing, JOM 69 (2017) 402–408, https://doi.org/10.1007/s11837-016-2198-1.
9. C. Bemfica, V. Nascimento, E. Fessler, J.A Araújo, F. Castro, Multiaxial fatigue of Inconel 718 produced by selective laser melting at room and high temperature, Int. J. Fatigue 163 (2022) 107108, https://doi.org/10.1016/j.ijfatigue.2022.107108.
10. H. Soni, M. Gor, G.S. Rajput, P. Sahlot, A comprehensive review on effect of process parameters and heat treatment on tensile strength of additively manufactured Inconel-625, Mater. Today 47 (2021) 4866–4871, https://doi.org/10.1016/j.matpr.2021.06.126.
11. E. Hosseini, V.A. Popovich, A review of mechanical properties of additively manufactured Inconel 718, Addit. Manuf. 30 (2019) 100877, https://doi.org/10.1016/j.addma.2019.100877.
12. R.R. Srivastava, M.S. Kim, J.C. Lee, M.K. Jha, B.S. Kim, Resource recycling of superalloys and hydrometallurgical challenges, J. Mater. Sci. 49 (2014) 4671–4686, https://doi.org/10.1007/s10853-014-8219-y.
13. A.B. Badiru, V.V. Valencia, A.B. Badiru, D. Liu, C.R. Hartsfield, A review on powder bed fusion technology of metal additive manufacturing. Additive Manufacturing Handbook, Product Development for the Defense Industry, (1st ed.). CRC Press. (2017) 251–61, https://doi.org/10.1201/9781315119106.
14. B.B. Milner, P. Gradl, G. Snedden, M. Brooks, J. Pitot, E. Lopez, M. Leary, F. Berto, A.d Plessis, Metal additive manufacturing in aerospace: A review, Mater. Des. 209 (2021) 110008, https://doi.org/10.1016/j.matdes.2021.110008.
15. N.J. Harrison, I. Todd, K. Mumtaz, Reduction of micro-cracking in nickel superalloys processed by Selective Laser Melting: A fundamental alloy design approach. Acta Mater. 94 (2015) 59–68, https://doi.org/10.1016/j.actamat.2015.04.035.
16. S. Herranz, F.J. Campa, L.N.L. Lacalle, A. Rivero, A. Lamikiz, E. Ukar, J.A. Sanchez, U. Bravo, The milling of airframe components with low rigidity: a general approach to avoid static and dynamic problems, Proc. IMechE Part B: J. Engineering Manufacture 219 (2005) 789-801, https://doi.org/10.1243/095440505X32742.
17. A. Mostafaei, R. Ghiaasiaan, I.T. Ho, S. Strayer, K.C. Chang, N. Shamsaei, S. Shao, S. Paul, A.C. Yeh, S. Tin, A.C. To, Additive manufacturing of nickel-based superalloys: A state-of-the-art review on process-structure-defect-property relationship, Prog. Mater. Sci. 136 (2023) 101108, https://doi.org/10.1016/j.pmatsci.2023.101108
18. E. Sadeghi, P. Karimi, R. Esmaeilizadeh, F. Berto, S. Shao, J. Moverare, E. Toyserkani, N. Shamsaei, A state-of-the-art review on fatigue performance of powder bed fusion-built alloy 718, Prog. Mater. Sci. 133 (2023) 101066, https://doi.org/10.1016/j.pmatsci.2022.101066
19. Md. Shahwaz, Pr. Nath, I. Sen, A critical review on the microstructure and mechanical properties correlation of additively manufactured nickel-based superalloys, J. Alloys Compd. 907 (2022) 164530, https://doi.org/10.1016/j.jallcom.2022.164530
20. G. Gudivada, A.K. Pandey, Recent developments in nickel-based superalloys for gas turbine applications: Review, J. Alloys Compd. 963 (2023) 171128, https://doi.org/10.1016/j.jallcom.2023.171128
21. Md. Shahwaz, Pr.Nath, I. Sen, Recent advances in additive manufacturing technologies for Ni-Based Inconel superalloys – A comprehensive review, J. Alloys Compd. 1010 (2025) 177654, https://doi.org/10.1016/j.jallcom.2024.177654
22. Q. Feng, Y. Wu, J. Li, Y. Cai, Y. Zhang, J. Liu, T. Liu, Effects of intermediate temperature on the grain boundary and γ’ precipitates of nickel-based powder superalloy under interrupted cooling, J. Alloy. Compd. 922 (2022) 166310, https://doi.org/10.1016/j.jallcom.2022.166310
23. F.G.L. Pereira, J.M. Lourenço, R.M. Nascimento, N.A. Castro, Fracture Behavior

and Fatigue Performance of Inconel 625, Mater. Res. 21(4) (2018) e20171089, https://doi.org/10.1590/1980-5373-MR-2017-1089.
24. H. Liu, H. Yu, C. Guo, X. Chen, S. Zhong, L. Zhou, A. Osman, J. Lu, Review on fatigue of additive manufactured metallic alloys: microstructure, performance, enhancement, and assessment methods, 30th Anniversary of City University of Hong Kong April 25, 36(17) (2024) 2306570. https://doi.org/10.1002/adma.202306570.
25. Y.L. Hu, Y.L. Li, S.Y. Zhang, X. Lin, Z.H. Wang, W.D. Huang, Effect of solution temperature on static recrystallization and ductility of Inconel 625 superalloy fabricated by directed energy deposition, Mater. Sci. Eng. A. 772 (2020), https://doi.org/10.1016/j.msea.2019.138711.
26. S.P. Kumar, S. Elangovan, R. Mohanraj, J.R. Ramakrishna, A review on properties of Inconel 625 and Inconel 718 fabricated using direct energy deposition, Mater. Today 46 (2021) 7892–7906, https://doi.org/10.1016/j.matpr.2021.02.566.
27. S.Y. Liu, S. Shao, H. Guo, R. Zong, C.X. Qin, X.Y. Fang, The microstructure and fatigue performance of Inconel 718 produced by laser-based powder bed fusion and post heat treatment, Int. J. Fatigue 156 (2022) 106700, https://doi.org/10.1016/j.ijfatigue.2021.106700.
28. T. Sugiyama, S. Utada, T. Yokokawa, M. Osawa, K. Kawagishi, S. Suzuki, H. Harada, Oxidation resistance improvement of Ni-Base single-crystal superalloy melted in a CaO crucible, Metall. Mater. Trans. A 50A (2019) 3903, https://doi.org/10.1007/s11661-019-05297-8.
29. Fatigue of Nikel-based supperalloys: Part Two, https://www.totalmateria.com/ru/articles/fatigue-of-nickel-based-superalloys-2/ (Accessed 19 April 2025).
30. Y. Wu, K. Sun, S. Yu, L. Zuo, Modeling the selective laser melting-based additive manufacturing of thermoelectric powders, Addit. Manuf. 37 (2021) 101666, https://doi.org/10.1016/j.addma.2020.101666.
31. N.A. Siddiqui, M. Muzamil, T. Jamil, G. Hussain, Heat sources in wire arc additive manufacturing and their impact on macro-microstructural characteristics and mechanical properties – An overview, Smart Mater. Manuf. 3 (2025) 100059, https://doi.org/10.1016/j.smmf.2024.100059.
32. Xi. Gong, T. Anderson, K. Chou, Review on powder-based electron beam additive manufacturing technology, Manufacturing Rev. 1(2) (2014) 1–12. https://doi.org/10.1051/mfreview/2014001.
33. Z. Tian, C. Zhang , D. Wang, W. Liu, X. Fang, D. Wellmann, Y. Zhao, Y. Tian, A review on laser powder bed fusion of Inconel 625 nickel-based alloy, Appl. Sci. 10(1) (2020) 81; https://doi.org/10.3390/app10010081.
34. I. Gibson, D. Rosen, B. Stucker, Additive Manufacturing Technologies, Springer New York, New York, 2015.
35. L.A Trejo, E.C. Urquizo, D. Bhate, A.R. Flores, Mechanical metamaterials with topologies based on curved elements: An overview of design, additive manufacturing and mechanical properties, Mater. Des. 233 (2023) 112190, https://doi.org/10.1016/j.matdes.2023.112190.
36. E.M. Sefene, State-of-the-art of selective laser melting process: A comprehensive review, J. Manuf. Syst. 63 (2022) 250–274, https://doi.org/10.1016/j.jmsy.2022.04.002.
37. A. Gisario, M. Kazarian, F. Martina, M. Mehrpouya, Metal additive manufacturing in the commercial aviation industry: A review, J. Manuf. Syst. 53 (2019) 124–149, https://doi.org/10.1016/j.jmsy.2019.08.005.
38. D. Svetlizky, M. Das, B. Zheng, A.L. Vyatskikh, S. Bose, A. Bandyopadhyay, J.M. Schoenung, E.J. Lavernia, N. Eliaz, Directed energy deposition (DED) additive manufacturing: Physical characteristics, defects, challenges and applications, 49 (2021) 271–295, https://doi.org/10.1016/j.mattod.2021.03.020.
39. Y. Li, C. Su, J. Zhu, Comprehensive review of wire arc additive manufacturing: Hardware system, physical process, monitoring, property characterization, application and future

prospects, Results in Eng. 13 (2022) 100330, https://doi.org/10.1016/j.rineng.2021.100330.
40. M. Liu, A. Kumar, S. Bukkapatnam, M. Kuttolamadom, A Review of the Anomalies in Directed Energy Deposition (DED) Processes & Potential Solutions - Part Quality & Defects, Procedia Manufacturing 53 (2021) 507–518, https://doi.org/10.1016/j.promfg.2021.06.093.
41. S. Suryakumar, K.P. Karunakaran, A. Bernard, U. Chandrasekhar, N. Raghavender, D. Sharma Weld bead modeling and process optimization in hybrid layered manufacturing, Comput. Aided Des. 43 (4) (2011) 331–344, http://dx.doi.org/10.1016/j.cad.2011.01.006.
42. D. Ding, Z. Pan, S.V. Duin, H. Li, C. Shen, Fabricating superior NiAl bronze components through wire arc additive manufacturing, Materials 9(8) (2016) 652, https://doi.org/10.3390/ma9080652.
43. N. Town, S. Lawler, 12 – Construction methods for small modular reactors (SMRs), Handbook of Small Modular Nuclear Reactors Woodhead Publishing Series in Energy 2015, 293–317, https://doi.org/10.1533/9780857098535.3.293
44. A. Ghorpade, U Prakash, S. Joshi, Effect of heat treatments on strengthening mechanisms in electron beam melted superalloy Inconel 718, Mater. Sci. Eng. A. 895 (2024) 146232, https://doi.org/10.1016/j.msea.2024.146232.
45. O. Gokcekaya, A. Günen, F. Ceritbinmez, A. Bahador, T. Nakano, M. Çetin, Wire-EDM performance and surface integrity of Inconel 718 with unique microstructural features fabricated by laser powder bed fusion, J. Adv. Manuf. Technol. (2024) 130 4513–4528, https://doi.org/10.1007/s00170-023-12924-7.
46. F.I. Jamhari, F.M. Foudzi, M.A. Buhairi, A.B. Sulong, N.A.M. Radzuan, N. Muhamad, I.F. Mohamed, N. Hani Jamadon, K.S. Seah, Influence of heat treatment parameters on microstructure and mechanical performance of titanium alloy in LPBF: A brief review, JMR&T. (2023) 24, 4091–4110, https://doi.org/10.1016/j.jmrt.2023.04.090.
47. A. Arghavan, K. Reza Kashyzadeh, A. Amiri Asfarjani, Investigating effect of industrial coatings on fatigue damage, Applied Mechanics and Materials. 87 (2011) 230-237, https://doi.org/10.4028/www.scientific.net/AMM.87.230.
48. K.R. Kashyzadeh, A. Arghavan, Study of the effect of different industrial coating with microscale thickness on the CK45 steel by experimental and finite element methods, Strength of materials. 45 (2013) 748-757, https://doi.org/10.1007/s11223-013-9510-x.
49. H. Abdollahnia, M.H. Alizadeh Elizei, K. Reza Kashyzadeh, Low-cycle fatigue behavior of H-shaped steel piles of an integral concrete bridge subjected to temperature variations, Materials Today: Proceedings. 46 (2021) 1657-1662, https://doi.org/10.1016/j.matpr.2020.07.261.
50. E. Maleki, K. Reza Kashyzadeh, Effects of the hardened nickel coating on the fatigue behavior of ck45 steel: experimental, finite element method, and artificial neural network modelling, Iranian Journal of Materials Science & Engineering. 14(4) (2017), https://doi.org/10.22068/ijmse.14.4.81.
51. K. Reza Kashyzadeh, E. Maleki, Experimental investigation and artificial neural network modeling of warm galvanization and hardened chromium coatings thickness effects on fatigue life of AISI 1045 carbon steel, Journal of Failure Analysis and Prevention. 17 (2017) 1276-1287, https://doi.org/10.1007/s11668-017-0362-8.
52. K.R. Kashyzadeh, S. Ghorbani, High-cycle fatigue behavior and chemical composition empirical relationship of low carbon three-sheet spot-welded joint: An application in automotive industry, Journal of Design Against Fatigue. 1(2) (2023) 1-8. https://doi.org/10.62676/p7x1cn02
53. N. Shamsaei, A. Yadollahi, L. Bian, S.M. Thompson, An overview of Direct Laser Deposition for additive manufacturing; Part II: Mechanical behavior, process parameter optimization and control, Addit. Manuf. 8 (2015) 12–35, https://doi.org/10.1016/j.addma.2015.07.002.
54. C.M. Pilgar, A.M. Fernandez, J. Segurado, Microstructure sensitive fatigue life prediction model for SLM fabricated Hastelloy-X, Int. J. Fatigue 168 (2023) 107372, https://doi.org/10.1016/j.ijfatigue.2022.107372.

55. A. Yadollahi, N. Shamsaei, Additive manufacturing of fatigue resistant materials: Challenges and opportunities, Int. J. Fatigue 98 (2017) 14–31, http://dx.doi.org/10.1016/j.ijfatigue.2017.01.001.
56. G. Macoretta, L. Bertini, B.D. Monelli, F. Berto, Productivity-oriented SLM process parameters effect on the fatigue strength of Inconel 718, Int. J. Fatigue 168 (2023) 107384, https://doi.org/10.1016/j.ijfatigue.2022.107384.
57. Y. Murakami, H. Masuo, Y. Tanaka, M. Nakatani, Defect analysis for additively manufactured materials in fatigue from the viewpoint of quality control and statistics of extremes, Procedia Struct. Integr. 19 (2019) 113–122, https://doi.org/10.1016/j.prostr.2019.12.014.
58. W. Li, T.Y. Hu, R. Sun, Y.C. Zhang, Effect of high temperature on failure behavior of additively manufactured superalloy under fatigue, Procedia Struct. Integr. 46 (2023) 119–124, https://doi.org/10.1016/j.prostr.2023.06.020.
59. I. Koutiri, E. Pessard, P. Peyre, O Amlou, T. Terris, Influence of SLM process parameters on the surface finish, porosity rate and fatigue behavior of as-built Inconel 625 parts, J. Mater. Process. Technol. 255 (2018) 536–546, https://doi.org/10.1016/j.jmatprotec.2017.12.043.
60. D.A. Maciel, Fatigue behaviour of Inconel 625 produced by directed energy deposition, Master's Thesis, Faculty of Engineering of the University of Porto, Porto, Portugal, 2020.
61. M.A. Anam, Microstructure and mechanical properties of selective laser melted superalloy inconel 625, PhD thesis, University of Louisville, 8 2018.
62. D.Z. Avery, O.G. Rivera, C.J.T. Mason, B.J. Phillips, J.B. Jordon, J. Su, N. Hard-wick, P.G. Allison, Fatigue behavior of solid-state additive manufactured inconel 625. JOM, 70 (2018) 2475–2484, https://doi.org/10.1007/s11837-018-3114-7.
63. D. Celli, M.H. Shen, T. George, O. Scott-Emuakpor, C. Holycross, Development of a fatigue damage and lifing assessment method for inconel 625 and aluminum 6061-T6. Turbo Expo: Power for Land, Sea, and Air, 2017. https://doi.org/10.1115/GT2017-63775.
64. A.E. Abela. High cycle fatigue of additively manufactured inconel 625. Master's thesis, Georgia Institute of Technology, 2020.
65. J.-R. Poulin, A. Kreitcberg, P. Terriault, V. Brailovski, Fatigue strength prediction of laser powder bed fusion processed Inconel 625 specimens with intentionally seeded porosity: Feasibility study, Int. J. Fatigue, 132 (2020) 105394. https://doi.org/10.1016/j.ijfatigue.2019.105394.
66. N. Kashaev, M. Horstmann, V. Ventzke, S. Riekehr, N. Huber, Comparative study of mechanical properties using standard and micro-specimens of base materials inconel 625, inconel 718 and Ti-6Al-4V, JMR 2(1) (2013) 41-47, http://dx.doi.org/10.1016/j.jmrt.2013.03.003.
67. G. Wu, M. Yang, Z. Yu, S. Zhang, H. Liu, J. Xiong, Experimental studies on the anisotropic fatigue behaviour of IN718 fabricated via wire arc additive manufacturing, Metals 14(7) (2024) 770, https://doi.org/10.3390/met14070770.
68. E. Salvati, A.J.G. Lunt, C.P. Heason, G.J. Baxter, A.M. Korsunsky, An analysis of fatigue failure mechanisms in an additively manufactured and shot peened IN 718 nickel superalloy, Mater. Des. 191 (2020) 108605, https://doi.org/10.1016/j.matdes.2020.108605.
69. A. Dinita, A. Neacs, A. Ileana Portoacă, M. Tănase, C. Nicolae Ilinca, I.N. Ramadan, Additive manufacturing post-processing treatments, a review with emphasis on mechanical characteristics, Materials (16) 2023 4610, https://doi.org/10.3390/ma16134610.
70. W. Wang, Z. Chen, W. Lu, F. Meng, T. Zhao, Heat treatment for selective laser melting of Inconel 718 alloy with simultaneously enhanced tensile strength and fatigue properties, J. Alloys Compd. 913 (2022) 165171, https://doi.org/10.1016/j.jallcom.2022.165171.
71. R. Konecna, L. Kunz, G. Nicoletto, A. Baca, Long fatigue crack growth in Inconel 718 produced by selective laser melting, Int. J. Fatigue 92 (2016) 499–506,

http://dx.doi.org/10.1016/j.ijfatigue.2016.03.012.
72. P.D. Nezhadfara, A.S. Johnsonc, N. Shamsaei, Fatigue behavior and microstructural evolution of additively manufactured Inconel 718 under cyclic loading at elevated temperature, Int. J. Fatigue 136 (2020) 105598, https://doi.org/10.1016/j.ijfatigue.2020.105598.
73. D. Deng, R.L. Peng, H. Brodin, J. Moverare, Microstructure and mechanical properties of Inconel 718 produced by selective laser melting: Sample orientation dependence and effects of post heat treatments, Mater. Sci. Eng. A 713 (2018) 294–306, https://doi.org/10.1016/j.msea.2017.12.043.
74. V. Paranthaman, D. Poosapadi, A. Sailesh, V. Sharma, R. Singh, R.L. Babu, K.K. Arun, M. Ravichandra, T.S. Senthil, Role of heat treatment in enhancing microstructure and properties of Inconel 625 manufactured by directed energy deposition using wire arc, JALMES 9 (2025) 100147, https://doi.org/10.1016/j.jalmes.2024.100147.
75. L.E. Murr, E. Martinez, S.M. Gaytan, D.A. Ramirez, B.I. Machado, P.W. Shindo, J.L. Martinez, F. Medina, J. Wooten, D. Ciscel, U. Ackelid, R.B. Wicker, Microstructural architecture, microstructures, and mechanical properties for a nickel-base superalloy fabricated by electron beam melting, Metall. Mater. Trans. A 42, 3491–3508 https://doi.org/10.1007/s11661-011-0748-2.
76. Y. Hu, X. Lin, Y. Li, S. Zhang, Q. Zhang, W. Chen, W. Li, W. Huang, Influence of heat treatments on the microstructure and mechanical properties of Inconel 625 fabricated by directed energy deposition, Mater. Sci. Eng. A 817 (2021) 141309, https://doi.org/10.1016/j.msea.2021.141309.
77. A.N.M. Tanvir, M.D.R.U. Ahsan, G. Seo, J.D. Kim, C. Ji, B. Bates, Y. Lee, D.B. Kim, Heat treatment effects on Inconel 625 components fabricated by wire + arc additively manufacturing (WAAM)—part 2: mechanical properties, J. Adv. Manuf. Technol. 110 (2020) 1709–1721, https://doi.org/10.1007/s00170-020-05980-w.
78. G.M. Volpato, U. Tetzlaff, M.C. Fredel, A comprehensive literature review on laser powder bed fusion of Inconel superalloys, Addit. Manuf. 55 (2022) 102871, https://doi.org/10.1016/j.addma.2022.102871.
79. R.M. Karimbaev, Y.S. Pyun, A. Amanov, Fatigue life extension of additively manufactured Nickel-base 718 alloy by nanostructured surface, Mater. Sci. Eng. A 831 (2022) 142041, https://doi.org/10.1016/j.msea.2021.142041.
80. X. Yin, X. Li, Y. Liu, D. Geng, D. Zhang, Surface integrity and fatigue life of Inconel 718 by ultrasonic peening milling, JMRT 22 (2023) 1392–1409, https://doi.org/10.1016/j.jmrt.2022.12.019.
81. D.A. Lesyk, S. Martinez, B.N. Mordyuk, V.V. Dzhemelinskyi, A. Lamikiz, G.I. Prokopenko, Pos t-processing of the Inconel 718 alloy parts fabricated by selective laser melting: Effects of mechanical surface treatments on surface topography, porosity, hardness and residual stress Surf. Coat. Technol. 381 (2020) 125136, https://doi.org/10.1016/j.surfcoat.2019.125136.